Development of bioluminescent Switchbody, antigen-triggered enzyme switch and elucidation of its principle

Takanobu Yasuda[1], Yoshiyuki Ueno[2], Masahiko Taguchi[3], Naoya Tochio[4], Hiromasa Yagi[4], Shuma Yazaki[5], Ryoichi Arai[5, 6], Bo Zhu[1], Takanori Kigawa[4], Hiroshi Ueda[1†] and Tetsuya Kitaguchi[1*]

[1]*Laboratory for Chemistry and Life Science, Institute of Integrated Research, Institute of Science Tokyo, Yokohama, 226-8501 Japan*
[2]*Graduate School of Life Science and Technology, Institute of Science Tokyo, Yokohama, 226-8501 Japan*
[3]*Institute of Multidisciplinary Research for Advanced Materials, Tohoku University, Sendai, 980-8577 Japan*
[4]*RIKEN Center for Biosystems Dynamics Research, Laboratory for Cellular Structural Biology, Yokohama, 230-0045 Japan*
[5]*Department of Applied Biology, Faculty of Textile Science and Technology, Shinshu University, Ueda, 386-8567 Japan*
[6]*Department of Biomolecular Innovation, Institute for Biomedical Sciences, Interdisciplinary Cluster for Cutting Edge Research, Shinshu University, Matsumoto, 390-8621 Japan*

[†]Deceased 23 December, 2022
*Corresponding author

Email: kitaguct-gfp@umin.ac.jp

Keywords: protein switch, homogeneous immunoassay, X-ray structural analysis, solution NMR, MD simulation

Abstract

We developed an enzyme switch, Switchbody, by integrating an antibody with a fragment of a split enzyme for precise enzyme activity regulation in response to an antigen. Using NanoLuc luciferase as the split enzyme, we engineered a luciferase-based Switchbody by fusing its fragment, HiBiT, to the N-terminus of antibody, and the Switchbody detected antigens in a dose-dependent manner with the complementary fragment, LgBiT, and its substrate. ELISA showed that interaction between HiBiT and LgBiT was enhanced by antigen binding. Moreover, X-ray crystallography and NMR revealed the heterogeneous trapped state of the HiBiT region and increased motility upon antigen binding, respectively. MD simulations and luminescence measurements showed that antigen disrupted the trapping of HiBiT in the antibody, enabling its release. By applying this "Trap & Release" principle to Protein M, an antibody binding protein, we successfully converted label-free IgG antibodies into bioluminescent immunosensors, demonstrating its versatility. The principle in Switchbody has the potential to expand switching technology beyond luciferase to other various enzymes in the future.

Introduction

Proteins exhibit dynamic structural changes in response to various external stimuli, including ligand binding, alterations in membrane potential, fluctuations in pH and temperature, as well as post-translational modifications, orchestrating various cellular physiological functions such as metabolism, signal transduction, and cytoskeletal reorganization. In other words, proteins work as molecular switches that dynamically respond to external stimuli. Therefore, by artificially manipulating the on/off states of protein precisely like a switch, these cellular physiological functions can be controlled as desired or visualized at high spatiotemporal resolution[1,2].

Several protein-based switches have been engineered to manipulate their activity by external stimuli. Examples include light-sensitive LOV2 domain of *Avena Sativa* phototropin 1 (AsLOV2) fusion protein to control effector access to protein of interest[3-5], designer receptors exclusively activated by designer drugs (DREADD) to activate G protein-coupled receptor (GPCR) with synthetic ligand[6,7], the Tet-on/off system to precisely regulate gene expression[8], FKBP-FRB dimerization by rapamycin to induce cooperative and hierarchical function of proteins[9,10], and fluorescent protein-based biosensor using protein-protein interaction[11,12] or conformational change[13,14] to visualize dynamics of target molecule. Although these switches are widely used and successful in applications such as controlling cellular physiological functions, molecular imaging, and diagnostics, their limitation lies in the inability to accommodate own selection of stimuli because the switch region of protein usually depends on the stimuli it originally receives.

To address this limitation, protein switches employing antibodies have been developed. The ability to produce antibodies recognizing targeted molecules and carry the high affinity and specificity for antigens make them ideal as switch components. Several advanced antibody-based switches have been reported, including chimeric antigen receptor (CAR) to cancer treatment[15], target-dependent RNA polymerase (TdRNAP) to transcriptional regulation in response[16], and antibody-based homogeneous biosensors to applications such as in situ immunoassays[17-19], monitoring protein production[20], and live-cell imaging[21-23].

On the other hand, split enzymes frequently serve as the functional domains driving the output of these antibody-based switches. To date, these antigen-triggered enzyme switches were engineered by being integrated with various split enzymes such as RNA polymerase[16], β-

galactosidase[24], β-lactamase[25,26], and luciferase[19,27,28] with antibodies, allowing to not only control transcription but also quantify antigen concentration through colorimetric or bioluminescence reaction using reconstitution of split enzymes induced by antigen-antibody binding. However, the reconstitution of split enzymes typically requires either the use of two antibodies or the antigen-induced association of VH and VL domains. Since successful reconstitution needs precise control over protein concentrations, binding orientation, and the spatial distance between the two protein components, we hypothesized that split enzyme reconstitution triggered by antigen binding to a single antibody would be a viable strategy to overcome these challenges.

During the attempts to develop a luciferase-based protein switch utilizing a distinct working principle, we accidentally discovered a bioluminescence increase of an antibody fragment scFv, which conjugated with the 11 amino acid HiBiT fragment derived from split NanoLuc[29] at a specific position of antibody, in the presence of LgBiT and its substrate, by the addition of antigen. We exploit the concept of this discovery, and successfully developed HiBiT fused antibody fragment, bioluminescent Switchbody, an enzyme switch that "Trap" HiBiT in antibody fragment and "Release" upon antigen binding (Fig. 1A), which was revealed by ELISA, X-ray crystallographic analysis, NMR and molecular dynamics simulations. Furthermore, we developed antibody binding protein M (PM)[30]-based probe carrying HiBiT, also successfully converted commercially available antibodies such as anti-TARGET-tag IgG and anti-Thyroxine IgG into enzyme switches, leading to bioluminescent enzyme switch recognizing a myriad of molecules. The innovative principle of the enzyme switch, in which a fragment derived from luciferase are trapped in antibodies and released it upon antigen binding, holds the potential to revolutionize immunoassays with multiplex detection through distinct enzymes and substrates, controlling various cellular physiological functions, as well as next-generation drug delivery systems with precise regulation of the timing and location of therapeutic release.

Results

Preparation of HiBiT fused anti-BGP scFvs, Switchbodies. To investigate whether conjugation of HiBiT fragment consisting of 11 amino acids in the vicinity of antigen binding site of antibody results in antigen-dependent bioluminescence increase, we prepared scFvs fused with HiBiT at the N-terminus via either a G_3S or $(G_3S)_2$ linker (Fig. 1B). Different linker lengths are generally tried during optimizing biosensors. As the model antibody, we employed the scFv fragment of anti-human osteocalcin (Bone Gla Protein, BGP) antibody, KTM219[31] because we are familiar with the properties and crystal structure of the antibody[17]. When the scFv and these HiBiT fused scFvs named Switchbodies were expressed in the *Escherichia coli* and purified, we found that expected bands of scFv, Switchbody (L1) carrying G_3S linker and Switchbody (L2) carrying $(G_3S)_2$ linker by SDS-PAGE analysis (Fig. 1C). Then, we performed ELISA to confirm the antigen-binding activity of recombinant scFv and Switchbodies. Switchbodies showed slightly lower binding activity compared to scFv (Fig. 1D), suggesting that HiBiT is located at the vicinity of antigen binding site and obstructs antigen binding by the steric hindrance, which is a desirable property for an antigen-dependent bioluminescent immunosensor. The purified Switchbodies were ready for validation of antigen-dependent bioluminescence.

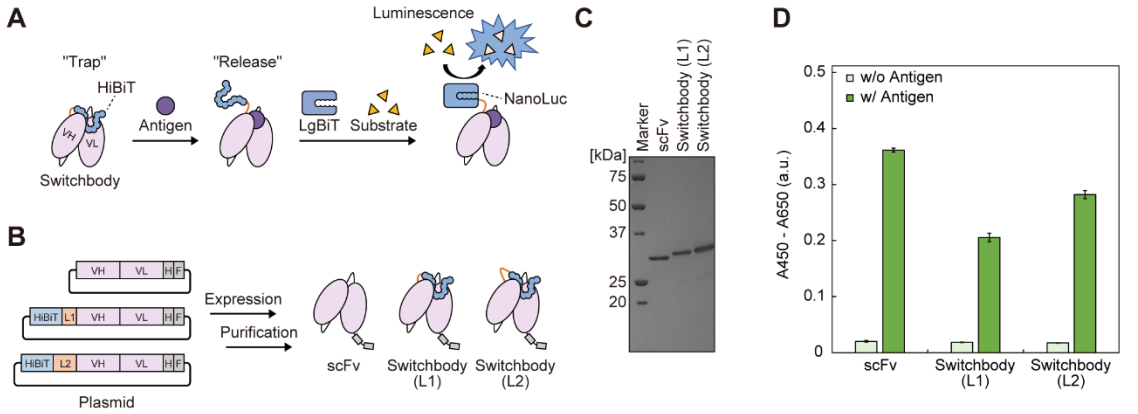

Fig. 1 Design and fabrication of Switchbody. (**A**) Concept of antigen detection by Switchbody. (**B**) Schematic illustration of the fabrication process for scFv and Switchbodies. L1: (G_3S) linker, L2: $(G_3S)_2$ linker, H: 6×His-tag, F: FLAG-tag. (**C**) SDS-PAGE analysis of purified scFv and Switchbodies. (**D**) Binding activity of scFv and Switchbodies to immobilized antigen, BGP-C11 examined by ELISA. Data are shown as mean ± standard deviation of triplicates. a.u.: arbitrary unit.

Luminescence of Switchbodies was increased by addition of antigen. The luminescence intensity of Switchbodies carrying different linker lengths with LgBiT and substrate was measured with or without antigen (Fig. 2A). While both Switchbodies showed increase in luminescence intensity over 3-fold with antigen BGP-C7 (NH_2-RRFYGPV-COOH), luminescence intensity with BGP-C10dV (NH_2-FQEAYRRFYGP-COOH) which lacks the C-terminal valine as a negative control was comparable to that without antigen. The luminescence intensity of both Switchbodies against antigen was increased in a dose-dependent manner (Fig. 2B). Then, the maximum responses, EC_{50}, and LOD of the Switchbody (L1) were 3.5-fold, 3.3 nM, and 0.32 nM, and that of Switchbody (L2) were 4.0-fold, 10 nM, and 1.2 nM, respectively (Supplementary Table 1). These EC_{50}, which are apparent K_D values, were consistent with the K_D values, 4.8 nM of the model antibody, KTM219[32]. Strikingly, the increase in luminescence intensity of Switchbody (L1) was recognized by a digital camera and even naked eye in a dark room (Supplementary Fig. 1). Furthermore, the luminescence intensity of Switchbodies against antigen was also increased in a dose-dependent manner in PBST containing body fluid such as human serum and plasma, and responses were larger than in PBST only (Fig. 2C, D). This larger response is consistent with that of our previous results, in which crowding effects caused by impurities such as proteins and lipids[33-35]. As the working principle of the Switchbody, we considered that upon antigen binding to scFv region of the Switchbody, a trapped HiBiT is released from the scFv and interact with LgBiT, leading to the reconstitution of NanoLuc and the emission of bioluminescence. To verify the HiBiT release, we examine the antigen-dependent binding of Switchbody to immobilized LgBiT by ELISA (Fig. 2E). As expected, the absorbance was increased in a dose-dependent manner, suggesting that antigen binding facilitate release of HiBiT from scFv leading to access to LgBiT.

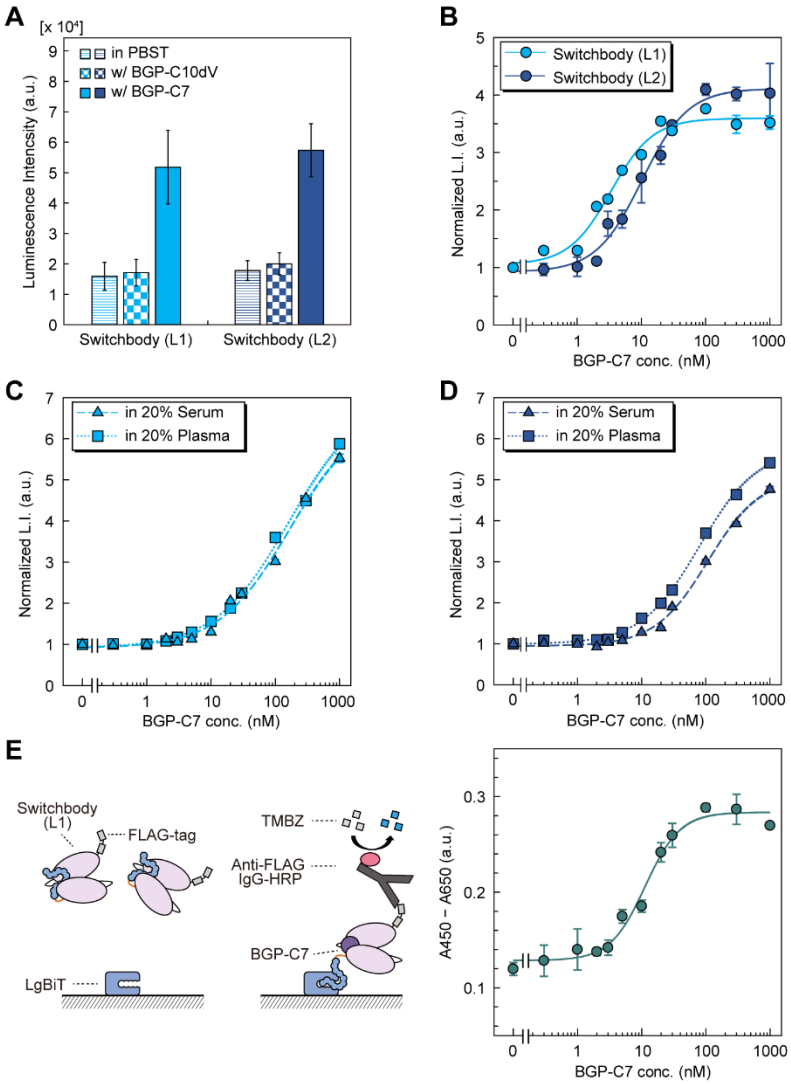

Fig. 2 Characterization of Switchbodies. (**A**) Luminescence response of 5 nM Switchbodies with 1 μM BGP-C10dV or BGP-C7. (**B–D**) Dose-response curve of 5 nM Switchbodies in PBST (pH 7.4, 0.1% Tween20) or 20% human serum or 20% human plasma. L.I.: luminescence intensity. (**E**) Antigen-dependent binding activity of Switchbody (L1) to immobilized LgBiT examined by ELISA. Data are shown as mean ± standard deviation of triplicates. a.u.: arbitrary unit.

Understanding HiBiT behavior in Switchbody by X-ray structural analysis. To obtain structural insights into the trapping mechanism of HiBiT, we solved the X-ray structure of Switchbody. The crystal of Switchbody based on KTM219 Fab, belonged to the orthorhombic space group $P2_12_12$, with unit cell constants of a = 95.84 Å, b = 65.91 Å, c = 69.56 Å, and contained one Switchbody comprising heavy chain fragment and light chain per asymmetric unit. The structure was refined to 1.95 Å resolution (R_{work} = 20.2%, R_{free} = 23.8%). All refinement statistics are shown in Supplementary Table 2. While the structure of Switchbody was solved (PDB ID: 9LUK), the N-teminal HiBiT region was disordered because its electron density was not visible, suggesting that heterogeneous state of HiBiT in Switchbody. Compared to the structure of Fab alone, which has been previously solved (PDB ID: 5X5X)[36], the atomic fluctuations based on the *B*-factor in the heavy chain complementarity-determining regions (CDRs) of the Switchbody were relatively larger (Fig. 3A, B). Moreover, structural conformations of these heavy chain CDRs differed considerably between Switchbody and Fab alone, compared to light chain CDRs and both chain framework regions (FRs) (Fig. 3C). These results suggest that the HiBiT did not tightly bind to specific site of the antibody in the absence of antigen, which is similar behavior with a fluorescent dye TAMRA in Q-body[36,37].

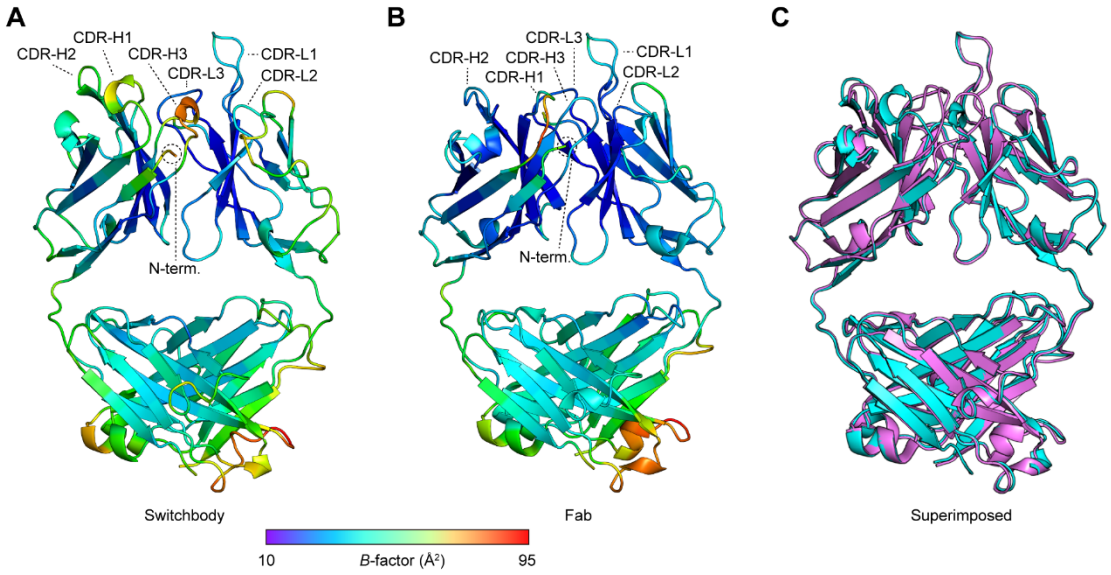

Fig. 3 Comparison of X-ray structures of Fab with and without HiBiT. (**A, B**) Ribbon representation of currently solved Switchbody structure (PDB ID: 9LUK) and previously solved Fab structure (PDB ID: 5X5X). These ribbon color represent the values of their *B*-factor as indicated in the scale bar. (**C**) Superimposed structure of Switchbody in cyan and Fab in magenta.

Analysis of motility of HiBiT in Switchbody by NMR. To investigate dynamics of Switchbody, especially HiBiT, in the absence or presence of antigen, we performed an NMR, which provides information on the dynamics of proteins in solution. We focused on the region around ^{1}H 10ppm, ^{15}N 130ppm where the signal derived from NH of the tryptophan (Trp) side chain is generally observed[38-40] because the HiBiT contains one Trp. Incidentally, the scFv contains totally five Trps, four Trps in VH and one Trp in VL (Fig. 4A). When ^{1}H-^{15}N HSQC spectra were measured, three signals (α–γ) and seven signals (a–e, x, and y) were observed for the Switchbody (L1) without and with antigen, respectively, on the region around ^{1}H 10ppm, ^{15}N 130ppm (Fig. 4B, Supplementary Fig. 2). The signal marked with asterisk is likely artifact such as aggregation and degradation by long-time analysis since the ^{1}H-^{15}N HSQC spectra showed the signal increased in a time-dependent manner (Supplementary Fig. 3). On the other hand, three signals without antigen (α–γ) were at positions similar to signals (α'–γ') and five signals with antigen (a–e) were similar to signals (a'–e') in the spectra of the scFv (Fig. 4C). We found significant differences upon adding antigen in the chemical shift, suggesting structural change of Switchbody (L1) and scFv induced by antigen binding. From the overlayed spectra of Switchbody (L1) and scFv in the presence of antigen, two signals x and y were observed in addition to signals (a–e) and (a'–e'), which were considered to be due to the fusion of HiBiT (Fig. 4D). Next, to quantitatively evaluate the dynamics of the HiBiT of the Switchbody (L1), we measured the transverse relaxation time T_2 for the Switchbody (L1) with antigen and estimated the transverse relaxation rate constant R_2 (s^{-1}). The R_2 of signal y was comparable to that of signals (a–e) (Fig. 4E, F, and Supplementary Table 3), while that of signal x was clearly smaller than those of other signals, suggesting that signal y is derived from Trp in the scFv region of Switchbody (L1) interacting with HiBiT, and that signal x was other than scFv region or scFv region changed its motility. Considering also that the appearance of signal x is after the addition of antigen, signal x is thought to be derived from a single Trp present in HiBiT, which increases motility upon antigen binding.

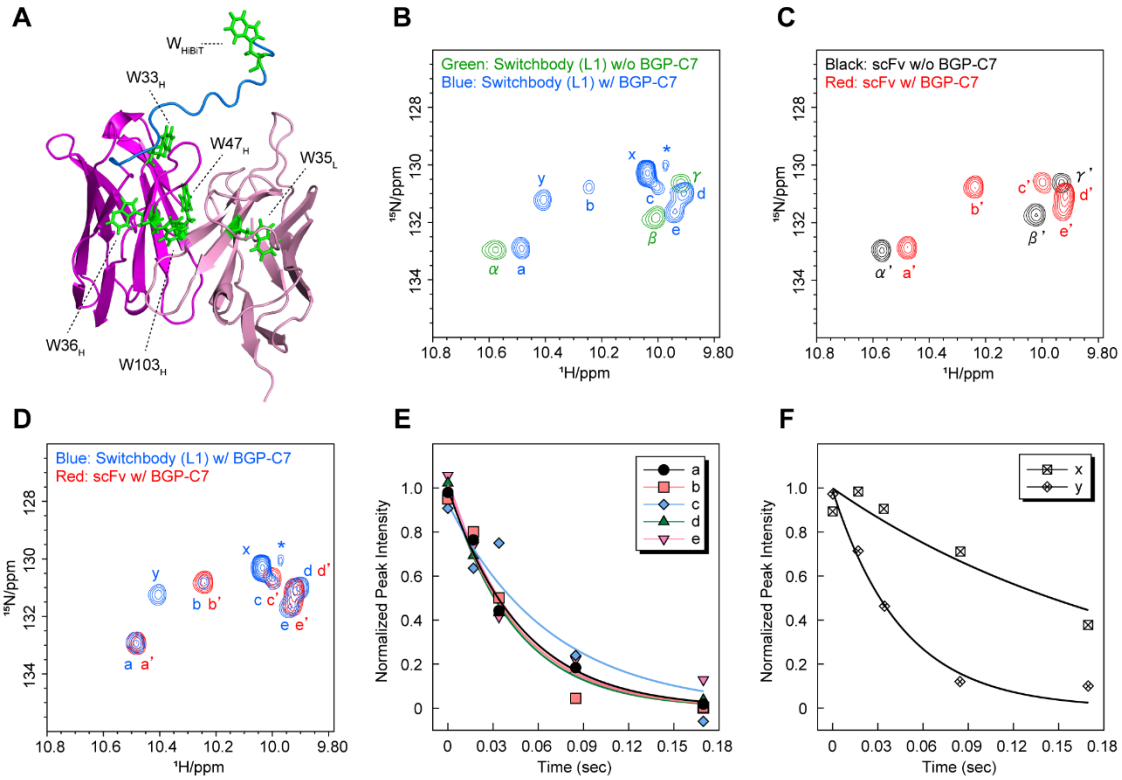

Fig. 4 The dynamic behavior of Switchbody with and without antigen by NMR. (**A**) Model structure of Switchbody (L1) generated from the crystal structure (PDB ID: 5X5X). HiBiT is shown in blue, VH in magenta, VL in pink, and Trp in green. (**B–D**) Overlay of ^{1}H-^{15}N HSQC spectra: Switchbody (L1) with and without antigen, scFv with and without antigen, Switchbody (L1) with antigen and scFv with antigen. (**E, F**) Transverse relaxation time T_2 for the Switchbody (L1) with antigen.

"Trap & Release" principle of Switchbody predicted by MD simulations. To understand further details about the working principle of Switchbody, we predicted an interaction between the HiBiT and scFv by molecular dynamics (MD) simulations. As initial model structures of Switchbody based on scFv were generated from the crystal structure (PDB: 5X5X for without antigen, PDB: 8XS1 for with antigen)[36] and MD simulations were performed for 3.0 μs with five independent runs. For analysis, the last 2.0 μs trajectories were used (total 10 μs for each) (Supplementary Movies 1, 2). Although HiBiT interacted in the vicinity of the antigen binding site, particularly heavy chain CDRs, in the absence of antigen, was moved out of the antigen binding site in the presence of antigen (Fig. 5A, B). To investigate which amino acid residues of HiBiT and scFv interact with each other, a contact frequency between the HiBiT and scFv was calculated using extracted 10,000 frames of MD simulations (Supplementary Tables 4, 5). The contact frequency was defined as the ratio of the number of frames in which the side chain of each amino acid residue was within 2.5 Å. A different contact map was created using values by subtracting the contact frequency with antigen from without antigen. In the absence of antigen, HiBiT frequently interacted with CDR-H1, H2, FR-H3, and CDR-L3, while CDR-H3, CDR-L1, and CDR-L2 in the presence of antigen (Fig. 5C). These results predict that the position of scFv interacting with HiBiT changes markedly before and after antigen binding. To validate the predictions of amino acid in scFv important for trapping HiBiT, we prepared eight alanine (Ala) mutants of Switchbody from the top ten most frequently contacted pairs, which are eight positions of scFv (Supplementary Fig. 4), and examined these binding of mutants to immobilized LgBiT by ELISA. In the absence of antigen, the mutants $W33_{H}A$, $D52_{H}A$, $D54_{H}A$, $S97_{H}A$ and $Y96_{L}A$ showed significantly higher absorbance signals compared to the original Switchbody (Fig. 5D), suggesting that the interaction HiBiT to scFv was weakened in four mutants by Ala mutation, making it easier to reconstitute with LgBiT. As expected, the four mutants showed higher luminescence than the original Switchbody without antigen (Fig. 5E), and the luminescence intensity was increased in a dose-dependent manner (Fig. 5F). These results imply that $W33_{H}$, $D52_{H}$, $D54_{H}$, $S97_{H}A$, and $Y96_{L}$ of KTM219 were important for the "Trap & Release" of the HiBiT.

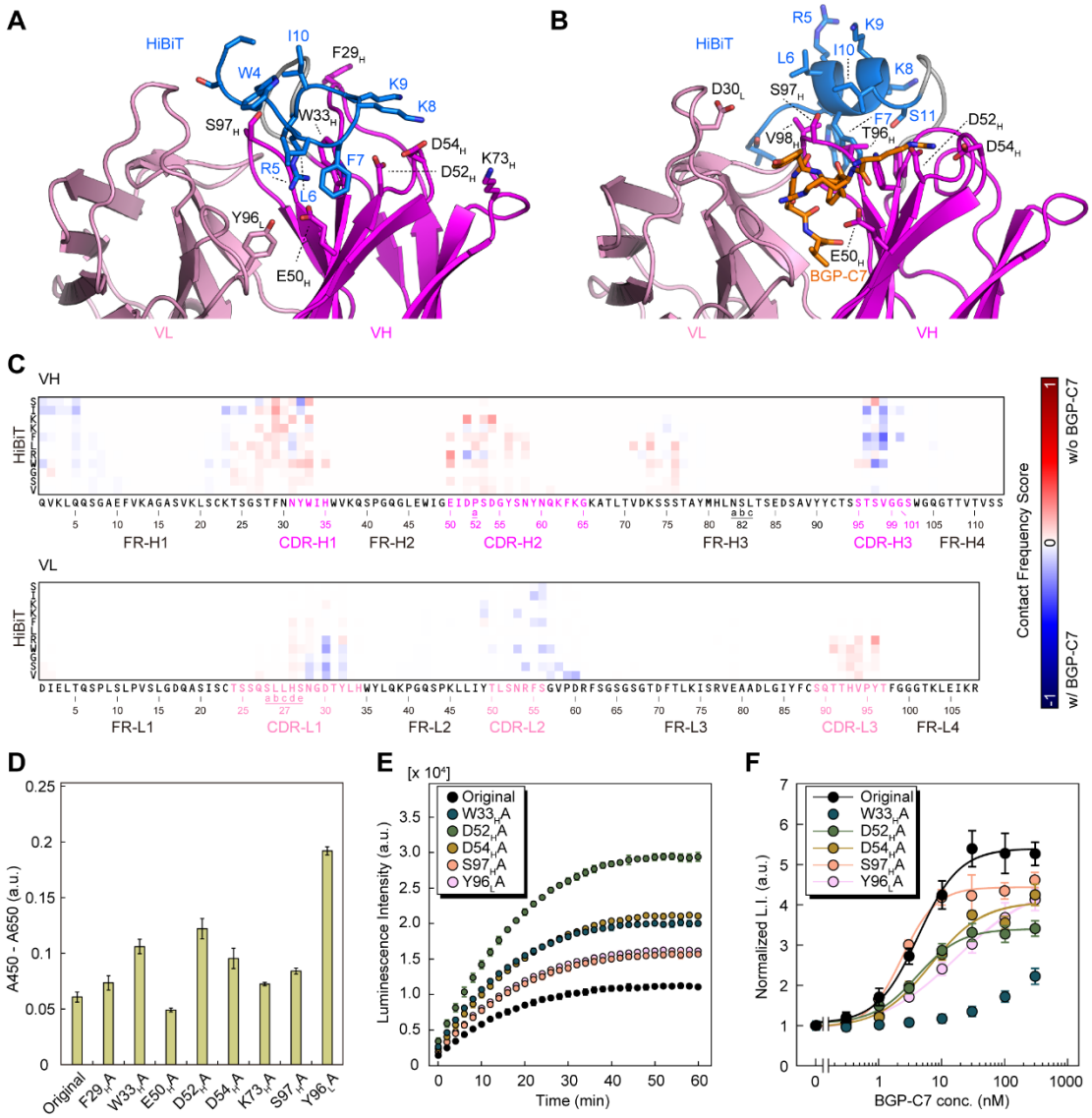

Fig. 5 Prediction of key amino acids on the antibody for "Trap & Release" of the HiBiT by MD simulations and its experimental validation. (**A, B**) Close-up view of antigen binding site of Switchbody generated by MD simulation. HiBiT is shown in blue, VH in magenta, VL in pink, and antigen peptide BGP-C7 in orange. (**C**) Heatmap showing the contact frequency between HiBiT and VH or VL region derived from MD simulation. FR and CDR region were defined by Kabat numbering. (**D**) Binding activity of Switchbody mutants to immobilized LgBiT examined by ELISA. W33$_H$A, D52$_H$A, D54$_H$A, S97$_H$A, and Y96$_L$A were significantly higher than the original according to Dunnett's test. p<0.05. (**E**) Time-course luminescence intensity for Switchbody mutants in the absence of antigen. (**F**) Dose-response curve of 1 nM Switchbody mutants in PBST (pH 7.4, 0.1% Tween20). Data are shown as mean ± standard deviation of triplicates. L.I.: luminescence intensity. a.u.: arbitrary unit.

Conversion of label-free IgGs into Switchbodies by antibody binding protein. We expected that increase of bioluminescence increases due to the "Trap & Release" of the HiBiT was widely applicable to various antibodies. To efficiently investigate antibodies without genetic manipulation, we prepared HiBiT fused antibody binding probe based on Protein M (PM) derived from *Mycoplasma genitalium*[30]. The concept is to convert antibodies into bioluminescent Swtichbodies by taking advantage of PM to bind most of the light chain of antibodies from many species with a high affinity at low nanomolar (Fig. 6A, B). When we prepared the PM-HiBiTs carrying various length linker (L0–3) for optimization (Supplementary Fig. 5A), we found expected bands of PM and PM-HiBiTs by SDS-PAGE analysis (Supplementary Fig. 5B), and binding activity to mouse polyclonal IgG was similar to that of PM alone (Supplementary Fig. 5C). To determine the suitable linker length between the PM and HiBiT to obtain a large response, PM-HiBiTs (L0–L3) were mixed with one model antibody, anti-BGP IgG KTM219, and two commercially available antibody, anti-Thyroxine IgG and anti-TRGET-tag IgG, and the luminescence intensity was measured with or without antigen. PM-HiBiT (L2) showed the largest response complexed with anti-Thyroxine IgG, and PM-HiBiT (L3) with anti-BGP IgG and anti-TRGET-tag IgG (Supplementary Fig. 5D–F, Supplementary Table 6), and luminescence for PM-HiBiTs/IgGs complex with antigens was increased in a dose-dependent manner (Fig. 6C–E, Supplementary Table 7). These results suggest that many commercially available antibodies are converted into immunosensors using PM-HiBiTs, leading to versatility of "Trap & Release" of HiBiT.

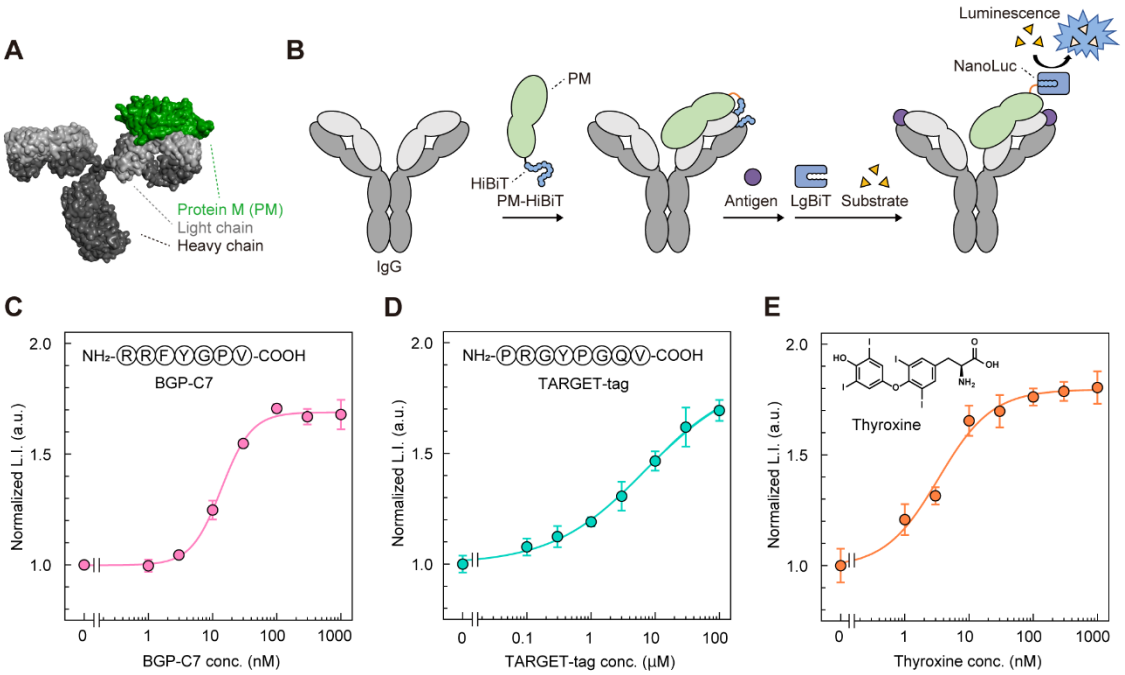

Fig. 6 Fabrication of label-free IgG based Switchbodies using antibody binding protein. (**A**) Model structure of Protein M/IgG complex generated from the crystal structure (PDB ID: 4NZR and 1IGT). (**B**) Concept of antigen detection using PM-HiBiT. (**C–E**) Dose-response curve of complexes of 1 nM PM-HiBiT and 5 nM IgG in PBST (pH 7.4, 0.1% Tween20): PM-HiBiT (L3)/KTM219 against BGP-C7, PM-HiBiT (L3)/P20.1 against TARGET-tag, PM-HiBiT (L2)/ME.125 against thyroxine. Data are shown as mean ± standard deviation of triplicates. L.I.: luminescence intensity. a.u.: arbitrary unit.

Discussion

In the present study, we discovered trap of 11 amino acids of HiBiT in the vicinity of antigen binding site of an antibody and its release respond to antigen, demonstrating that this mechanism enables us to develop a luciferase-based protein switch, bioluminescent Switchbody.

The absorbance in the ELISA with immobilized antigen was marginally higher for Switchbody (L2) compared to Switchbody (L1) (Fig. 1D), implying Switchbody (L2) is more likely to bind to the antigen due to the extended linker length. Since the antibody region is the same for Switchbody (L1) and (L2), this is not caused by the change in affinity between antibody and antigen. Instead, it would be attributed to the position of HiBiT fused to Switchbody (L2) being slightly distant from the antigen binding site due to the linker being too long, leading to easier access of antigen to antibody. Accordingly, the Switchbody (L2) requires more antigen to release the trapped HiBiT, and the EC_{50} of Switchbody (L2) was larger than Switchbody (L1) (Fig. 2B, Supplementary Table 1). Therefore, we believe that a linker length that allows HiBiT to be close to the antigen binding site is necessary to develop a Switchbody with a large response.

Regarding the detailed mechanism of HiBiT trapping to the antibody, through combining contact maps generated from MD simulation (Fig. 5C) with the X-ray structural analysis (Fig. 3) we can interpret the HiBiT interacts with multiple sites in the vicinity of heavy chain CDRs rather than tightly bind to specific site of the antibody. In particular, the MD simulations predicted the salt-bridge interactions between $D52_H$ or $D54_H$ residues of the scFv and K9 of HiBiT. The $D52_HA$ or $D54_HA$ mutants of Switchbody showed higher luminescence intensity compared to the original Switchbody in the absence of antigen (Fig. 5E), reflecting the weakening of the HiBiT trap in scFv due to destroying the salt-bridges to Lys by substitution of Asp for Ala. Therefore, one of the key mechanisms for "Trap & Release" of HiBiT would involve the interaction and antigen-dependent disruption of the salt-bridge between K9 of HiBiT and $D52_H$ and/or $D54_H$ of scFv. As interpreted above, given that HiBiT interacts with multiple sites on the antibody, it may be feasible to modulate the intensity and frequency of "Trap & Release" by selectively specific amino acid residues on the antibody for mutation, tailored to the intended application.

In fluorescent immunosensor Q-bodies, which we believe utilize the same "Trap & Release" principle, the fluorescent dyes such as TAMRA, ATTO520, R6G, etc. have also been shown to be trapped in the antibody via π-π stacking interaction between xanthene part of dye and side chain of Trp of antibody, and released upon antigen binding[37,41,42]. Since antigen-antibody interactions involve various molecular interactions, including hydrogen bonds, cation-π, and hydrophobic interactions in addition to salt-bridges and π-π stacking interactions[36,43,44], simply placing a short fragment in the vicinity of antigen binding site is likely to induce various molecular interactions. In fact, anti-TARGET-tag IgG, P20.1 was able to induce "Trap & Release" of HiBiT in an antigen-dependent manner despite the absence of $D52_H$ and $D54_H$, which is important for salt-bridge between HiBiT and anti-BGP antibody, KTM219. Therefore, not only dyes and fused fragments but various other compounds may be trapped in antibodies and released as a switch upon antigen binding.

In conclusion, we found that HiBiT region in Switchbody has increased motility and LgBiT accessibility in the presence of antigen, reflecting HiBiT trapped in the antibody is released from the antibody upon antigen binding. Then, leveraging this unique "Trap & Release" principle, we successfully developed a luciferase-based protein switch, bioluminescent Switchbody. This technology will extend beyond analysis and detection, and its advancement for intracellular application enables precise regulation of cellular physiological functions by antigen, utilizing fragments from split enzymes involved in key processes such as proliferation, differentiation, and metabolism. Furthermore, expanding the potential for therapeutic applications will facilitate targeted drug release, paving the way for treatments with enhanced target selectivity and minimized side effects.

Methods

Plasmid construction. The DNA fragments encoding the scFvs and Switchbodies were amplified via PCR and inserted into the pSQ vector[41], which was digested with NdeI and BamHI. The DNA fragment encoding the LgBiT was amplified via PCR and inserted into the pET-32b(+) vector, which was digested with NcoI and XhoI. The DNA fragments encoding the Protein M and PM-HiBiTs were amplified via PCR and the products were inserted into the pTrx'st2 vector[45], which was digested with NcoI and XhoI. PCR was performed using KOD-Plus-Neo (TOYOBO, #KOD-401). Amplified DNA insertion to each vector was performed using In-Fusion HD Cloning Kit (Takara Bio, #639649). All cloning results were confirmed by Sanger sequencing (Azenta). The amino acid sequences of all the proteins used in this study are listed in supplementary information (Supplementary Tables 9–11).

Protein preparation. Expression vector of the protein was transformed into *E. coli* SHuffle T7 Express *lys*Y competent cells (New England Biolabs, #C3030J). Cells were cultured in Luria-Bertani (LB) medium (Difco LB broth, Lennox, BD, #240230) containing 100 μg/mL ampicillin at 30°C to an OD_{600} = 0.4–0.6, then the expression was induced by 0.4 mM isopropyl β-d-thiogalactopyranoside (IPTG) and the culture was incubated for 16 h at 16°C. The cultured cells were collected by centrifugation at 8,000×g for 10 min at 4°C, and the pellet was resuspended in purification buffer (50 mM phosphate, 300 mM NaCl, pH 7.4). They were disrupted by a cell disruptor One shot model (Constant Systems), and the lysate was centrifuged at 8,000×g for 10 min at 4°C to collect the supernatant. The His-tagged protein in the supernatant was purified with TALON Metal Affinity Resin (Takara Bio, #635504) according to the manual and eluted into the elution buffer (50 mM phosphate, 300 mM NaCl, 500 mM Imidazole, pH 7.4). Then, the purified protein was buffer-exchanged to PBS (pH 7.4) using MicroSpin G-25 Columns (Cytiva, #27532501), and glycerol was added at a final concentration of 15% for long-term storage at -30°C. The purified proteins were analyzed by SDS-PAGE, and the concentration was determined by band intensity after Coomassie Brilliant Blue staining using bovine serum albumin as standards on the same gel.

For NMR studies, transformed *E. coli* SHuffle T7 Express *lys*Y competent cells were cultured in 5 mL LB medium containing 50 μg/mL ampicillin overnight at 37°C and subsequently cultured in 9 L M9 minimal medium containing 0.5 g/L $^{15}NH_4Cl$ for the selective ^{15}N-labeling at 37°C to an OD_{600} = 0.5–0.7 using JAR FERMENTOR MBF (TOKYO RIKAKIKAI). Then, expression was induced by 0.4 mM IPTG and the culture was incubated overnight at 16°C. The cultured cells were collected by centrifugation at 6,000 rpm for 10 min at 4°C, and the pellet was resuspended in purification buffer followed by disruption by sonication. After the suspension was centrifuged to collect the supernatant, proteins were purified using TALON Metal Affinity Resin according to the manual and eluted into the elution buffer. Then, the purified protein was buffer-exchanged to the purification buffer using PD-10 column (Cytiva, #17085101). The tag sequence at the N-terminal region of the protein was cleaved by 0.5 μM TEV protease with 1 mM DTT at room temperature overnight and subsequently removed from the protein using TALON Metal Affinity Resin. After buffer-exchange to 20 mM MES buffer (pH 6.0) containing 100 mM NaCl using a PD-10 column, proteins were further purified using a HiTrap SP HP cation exchange chromatography column (Cytiva, #17115201). The collected eluates were concentrated and buffer-exchanged to NMR buffer (20 mM Tris, 300 mM NaCl, 5% D_2O, pH 7.0) using a Vivaspin 2–10K (Cytiva, #28932247). Finally, approximately 200 μL of 259 μM ^{15}N-labeled Switchbody (L1) was obtained. Similarly, approximately 500 μL of 278 μM ^{15}N-labeled scFv was obtained from 4.4 L culture using a flask following the same procedure.

ELISA. For antigen immobilization, 10 μg/mL streptavidin in PBS (pH 7.4) was applied to a clear 96-well microplate (Greiner Bio-One, #655001) and incubated overnight at 4°C. After washing the plate three times with PBST (PBS containing 0.1% Tween20, pH 7.4), PBS (pH 7.4) containing 20% ImmunoBlock (KAC, #CTKN001), 1 μg/mL biotinylated human BGP-C11 peptide (Bio-QEAYRRFYGPV-COOH, LifeTein), 20 nM scFv or Switchbody, and 0.1 μg/mL anti-His IgG-HRP were successively added to the wells. Each reagent was incubated individually for 2 hours, 1 hour, 1 hour, and 30 minutes, respectively. After each incubation step, the wells were washed three times with PBST. Subsequently, a substrate solution (100 mM sodium acetate, 100 μg/mL TMBZ, 0.03% H_2O_2, pH 6.0) was applied and incubated for few minutes. The reaction was stopped with

10% H_2SO_4, and the absorbance was measured at 450 nm with a reference at 650 nm using a microplate reader SH-1000 (Corona Electric).

For LgBiT immobilization, 175 nM LgBiT in PBS (pH 7.4) was applied to a clear 96-well microplate and incubated overnight at 4°C. After washing the plate three times with PBST, PBS (pH 7.4) containing 20% ImmunoBlock, 1 nM Switchbody, and 0.1 μg/mL anti-FLAG IgG-HRP were successively added to the wells. Each reagent was incubated individually for 2 hours, 20 minutes, and 30 minutes, respectively. After each incubation step, the wells were washed three times with PBST. The subsequent procedure was the same as described above.

For mouse IgG immobilization, 10 μg/mL mouse IgG (FUJIFILM Wako, #140-09511) in PBS (pH 7.4) was applied to a clear 96-well microplate and incubated overnight at 4°C. After washing the plate three times with PBST, PBS (pH 7.4) containing 20% ImmunoBlock, 5 nM Protien M or PM-HiBiT, and 1/5000 diluted StrepTactin-HRP (Bio-Rad, #1610380) were successively added to the wells. Each reagent was incubated individually for 2 hours, 1 hour, and 30 minutes, respectively. After each incubation step, the wells were washed three times with PBST. The subsequent procedure was the same as described above.

Luminescence intensity measurement. Purified LgBiT and NanoGlo substrate (Promega, #N1110) were mixed at a final concentration of 1–5 nM and a 2000-fold dilution, respectively, and were applied to a white 96-well microplate (Greiner Bio-One, #675075). Separately, 1–5 nM Switchbody, pre-incubated with or without the antigen peptide (LifeTein) in PBST (pH 7.4) for 30 minutes at room temperature, was also applied to the white microplate. Immediately afterward luminescence intensity at 460 nm with a bandwidth of 30 nm was measured using a CLARIOstar (BMG LABTECH).

For measurements under crude condition, either human serum or human plasma was mixed to a final concentration of 20% in PBST during sample preparation. For PM-HiBiT assay, 1 nM PM or PM-HiBiT was incubated with 5 nM of each IgG: anti-BGP IgG (KTM219, lab-made), anti-TARGET-tag IgG (P20.1, FUJIFILM Wako, #016-25481), anti-thyroxine IgG (ME.125, Abnova,

#MAB4752). The incubation was performed in PBST (pH 7.4) for 40 minutes at room temperature before measurement.

Dose-response curve fitting. Dose-response curves were fitted to a four-parameter logistic equation as below using ImageJ 1.54i software (Wayne Rasband).

$$y = d + \frac{a - d}{1 + \left(\frac{x}{c}\right)^b}$$

The limit of detection was calculated as the concentration corresponding to the mean blank value plus three times its standard deviation.

Bioluminescence observation in camera. To observe and capture images of luminescence, 5 nM Switchbody (L1), 0.3, 2, 5, 20, 100, 1,000 nM BGP-C7, 5 nM LgBiT, and NanoGlo substrate at a final dilution of 1000-fold in PBST were added to a white 96-well microplate. Images were taken using a digital camera α7S (Sony) set at ISO 8000, F1/2, with a five seconds exposure in a dark room.

Crystallization experiments. The Fab-based Switchbody was purified using immobilized metal affinity chromatography with TALON Metal Affinity Resin, anion exchange chromatography with a RESOURCE Q 1 mL column (Cytiva, #17117701), and size-exclusion chromatography with a Superdex 75 Increase 10/300 GL column (Cytiva, #29148721), as previously described[36]. The 10 mg/mL protein was crystallized at 20°C using the hanging drop vapor diffusion method. The 1 μL Switchbody was mixed with the same volume of reservoir solution (0.1 M Bis-Tris, pH 6.0, 22% w/v polyethylene glycol monomethyl ether 2000).

Data collection, structure determination and refinement. X-ray diffraction data was collected at KEK Photon Factory (PF) Structural Biology Beamline BL-5A or AR-NW12A at 95 K with reservoir solution added to 25% w/v PEG 400 or 25% w/v glycerol as a cryoprotectant. Diffraction data was processed with the program XDS[46] and AIMLESS[47]. The structure was solved by molecular replacement method using Phaser with a model structure of anti-osteocalcin antibody

KTM219 (PDB ID: 5X5X)[36]. The structural model was corrected with the program COOT[48] and was refined with the program REFMAC5[49] in the CCP4 suite[50]. The quality of the model was inspected by the programs PROCHECK[51], RAMPAGE[52], and MolProbity[53]. All data collection and refinement statistics are shown in Supplementary Table 2. The atomic coordinates and the structure factors have been deposited in the Protein Data Bank (PDB) with the accession codes 9LUK. The graphic figures were created using the program PyMOL (Schrödinger).

Preparation of thermostable scFv for NMR study. Since high-concentration samples (> 200 μM) were required for NMR structural analysis, tyrosine at position 27 of the heavy chain in the scFv was mutated to serine to improve thermal stability. Initially, $F11_H$, $Y27_H$, $F29_H$, and $L9_L$ were selected as candidates for thermostable mutations based on computational predictions of sidechain solvent accessibility and hydrophobicity of the scFv, using Discovery Studio Visualizer v18.1 (BIOVIA) (Supplementary Fig. 6A, B). These selected hydrophobic amino acids were mutated to hydrophilic amino acids, either serine or threonine, and the antigen-binding activity of the mutants was evaluated by ELISA (Supplementary Fig. 6C). To assess the thermal stability of each mutant, the binding activity of the mutants to immobilized antigen after incubation at 60°C for various time was examined by ELISA. Among the wild-type and mutants, $Y27_HS$ mutant exhibited the longest half-time of binding activity after incubation at 60°C (Supplementary Fig. 6D, Supplementary Table 8). Consequently, we determined to use the $Y27_HS$ mutant for NMR study, MD simulation and subsequent luminescence intensity measurements.

NMR studies. The ^{1}H-^{15}N HSQC spectra were measured using an Avance III 700-MHz spectrometer (Bruker Biospin) at 298 K. The ^{15}N-labeled protein sample was dissolved in an NMR buffer (20 mM Tris, 300 mM NaCl, 5% D_2O, pH 7.0) at a concentration of 200 μM, either with or without 300 μM antigen BGP-C7. The interscan delay was set to 1.7 seconds, the number of data integrations was 32, and the number of data points were 1,024 pts [^{1}H] and 128 pts [^{15}N]. For the transverse relaxation time T_2 measurements, the delay intervals were set to 0, 17.0, 33.9, 84.8, and 169.6 ms. The apparent transverse relaxation rate constant R_2 was estimated by fitting peak

intensities using Monte Carlo method (N = 128) as a function of above 5 relaxation delay intervals based on the following equation.

$$I_{\mathrm{t}} = I_0 \cdot \mathrm{e}^{-\mathrm{t}\cdot R_2}$$

All NMR spectra were processed using TopSpin 3.6.2 software (Bruker Biospin).

System preparation for MD simulation. The initial simulation structures were constructed using X-ray crystallographic structures of Fab fragment (KTM219) with and without antigen (PDB ID: 5X5X and 8XS1) to match protein sequences used in the NMR experiment. Crystallographic water molecules within 5.0 Å from the extracted protein region are retained. Structures of HiBiT, linker between HiBiT and VH region, as well as one between VH and VL regions are modelled by MODELLER[54]. Missing hydrogen atoms were added to the protein with the LEaP module of AMBER20. The simulation systems were solvated with TIP3P water molecules[55] with a minimum distance of 15.0 Å between the protein and the box edges, and Na^+ and Cl^- ions were added to neutralize the systems and match condition in the NMR experiment (300 mM NaCl). The force field parameter set of AMBER ff14SB[56] and that reported in reference[57] were employed for the force fields of the protein, Na^+ and Cl^- ions, respectively. The total number of atoms in the box were 80,266 and 60,569 atoms for system with and without antigen.

MD simulation. GPU modules of the AMBER20 program package[58] were employed. The simulation systems were first subject to energy minimization under harmonic restraints to heavy atoms of the protein with a force constant of 5.0 kcal/(mol·Å^2). The structures were further energetically minimized under harmonic restraints to C_α atoms of the protein with a force constant of 5.0 kcal/(mol·Å^2). Next, the systems were heated from 0 K to 298 K for 300 ps in NVT condition under harmonic restraints of C_α atoms of the protein with a force constant of 5.0 kcal/(mol·Å^2). After the heating, the systems were gradually relaxed in NPT condition with decreasing the harmonic restraints to C_α atoms of the protein with a force constant of 5.0, 3.0, 2.0, 1.0, 0.5, 0.3, 0.2, and 0.1 kcal/(mol·Å^2) for every 1.0 ns. Then, five independent production runs at 298 K for 3.0 μs in NPT condition were performed. Long-range electrostatic interactions were calculated using the particle mesh Ewald method[59]. Temperature and pressure were controlled with Langevin

bath (collision frequency is 2.0 ps^{-1}) and Berendsen's methods. Nonbonded interactions were cut off at 8.0 Å, and bond lengths including hydrogen atoms were constrained by the SHAKE/RATTLE method[60]. The time step for integration was set to 2.0 fs. For analysis, the last 2.0 μs trajectories were used. The total MD trajectory for analysis is 10 μs for each system. Molecular figures were generated using the PyMOL Molecular Graphics System (Schrödinger).

Residue-wise contact map analysis. Contact map analysis was performed by MDTraj[61]. Residue-wise intra-contact was counted if any of side-chain atoms from a pair of residues is less than 2.5 Å. Then, differences of contacts were calculated by subtracting contacts of the system without antigen from those of the system with antigen.

References

1. Stein, V.& Alexandrov, K. Synthetic protein switches: design principles and applications. *Trends Biotechnol.* **33**, 101–110 (2015).

2. Alberstein, R. G., Guo, A. B.& Kortemme, T. Design principles of protein switches. *Curr. Opin. Struct. Biol.* **72**, 71–78 (2022).

3. Wu, Y. I. et al. A genetically encoded photoactivatable Rac controls the motility of living cells. *Nature* **461**, 104–108 (2009).

4. Strickland, D. et al. TULIPs: tunable, light-controlled interacting protein tags for cell biology. *Nat. Methods* **9**, 379–384 (2012).

5. Niopek, D. et al. Engineering light-inducible nuclear localization signals for precise spatiotemporal control of protein dynamics in living cells. *Nat. Commun.* **5**, 4404 (2014).

6. Armbruster, B. N., Li, X., Pausch, M. H., Herlitze, S.& Roth, B. L. Evolving the lock to fit the key to create a family of G protein-coupled receptors potently activated by an inert ligand. *Proc. Natl. Acad. Sci. USA* **104**, 5163–5168 (2007).

7. Bonaventura, J. et al. High-potency ligands for DREADD imaging and activation in rodents and monkeys. *Nat. Commun.* **10**, 4627 (2019).

8. Gossen, M.& Bujard, H. Tight Control of Gene-Expression in Mammalian-Cells by Tetracycline-Responsive Promoters. *Proc. Natl. Acad. Sci. USA* **89**, 5547–5551 (1992).

9. Dagliyan, O. et al. Rational design of a ligand-controlled protein conformational switch. *Proc. Natl. Acad. Sci. USA* **110**, 6800–6804 (2013).

10. Karginov, A. V. et al. Dissecting motility signaling through activation of specific Src-effector complexes (vol 10, pg 286, 2014). *Nat. Chem. Biol.* **10**, 692–692 (2014).

11. Miyawaki, A., Griesbeck, O., Heim, R.& Tsien, R. Y. Dynamic and quantitative Ca measurements using improved cameleons. *Proc. Natl. Acad. Sci. USA* **96**, 2135–2140 (1999).

12. Huppertz, M. C. et al. Recording physiological history of cells with chemical labeling. *Science* **383**, 890–897 (2024).

13. Nakai, J., Ohkura, M.& Imoto, K. A high signal-to-noise Ca probe composed of a single green fluorescent protein. *Nat. Biotechnol.* **19**, 137–141 (2001).

14. Arai, S. et al. RGB-Color Intensiometric Indicators to Visualize Spatiotemporal Dynamics of ATP in Single Cells. *Angew. Chem. Int. Ed.* **57**, 10873–10878 (2018).

15. Larson, R. C.& Maus, M. V. Recent advances and discoveries in the mechanisms and functions of CAR T cells. *Nat. Rev. Cancer* **21**, 145–161 (2021).

16. Komatsu, S., Ohno, H.& Saito, H. Target-dependent RNA polymerase as universal platform for gene expression control in response to intracellular molecules. *Nat. Commun.* **14**, 7256 (2023).

17. Abe, R. et al. "Quenchbodies": Quench-Based Antibody Probes That Show Antigen-Dependent Fluorescence. *J. Am. Chem. Soc.* **133**, 17386–17394 (2011).

18. Xue, L., Yu, Q. L. Y., Griss, R., Schena, A.& Johnsson, K. Bioluminescent Antibodies for Point-of-Care Diagnostics. *Angew. Chem. Int. Ed.* **56**, 7112–7116 (2017).

19. Ni, Y. et al. A plug-and-play platform of ratiometric bioluminescent sensors for homogeneous immunoassays. *Nat. Commun.* **12**, 4586 (2021).

20. Ito, Y. et al. Efficient Microfluidic Screening Method Using a Fluorescent Immunosensor for Recombinant Protein Secretions. *Small* **19**, 2207943 (2023).

21. Sato, Y. et al. Genetically encoded system to track histone modification. *Sci. Rep.* **3**, 2436 (2013).

22. Wongso, D., Dong, J., Ueda, H.& Kitaguche, T. Flashbody: A Next Generation Fluobody with Fluorescence Intensity Enhanced by Antigen Binding. *Anal. Chem.* **89**, 6719–6725 (2017).

23. Dai, Y. C. et al. Intra Q-body: an antibody-based fluorogenic probe for intracellular proteins that allows live cell imaging and sorting. *Chem. Sci.* **13**, 9739–9748 (2022).

24. Yokozeki, T., Ueda, H., Arai, R., Mahoney, W.& Nagamune, T. A homogeneous noncompetitive immunoassay for the detection of small haptens. *Anal. Chem.* **74**, 2500–2504 (2002).

25. Kojima, M. et al. Activation of Circularly Permutated β-Lactamase Tethered to Antibody Domains by Specific Small Molecules. *Bioconjug. Chem.* **22**, 633–641 (2011).

26. Iwai, H., Kojima-Misaizu, M., Dong, J. H.& Ueda, H. Creation of a Ligand-Dependent Enzyme by Fusing Circularly Permuted Antibody Variable Region Domains. *Bioconjug. Chem.* **27**, 868–873 (2016).

27. Stains, C. I. et al. A General Approach for Receptor and Antibody-Targeted Detection of Native Proteins Utilizing Split-Luciferase Reassembly. *ACS Chem. Biol.* **5**, 943–952 (2010).

28. Ohmuro-Matsuyama, Y.& Ueda, H. Homogeneous Noncompetitive Luminescent Immunodetection of Small Molecules by Ternary Protein Fragment Complementation. *Anal. Chem.* **90**, 3001–3004 (2018).

29. Dixon, A. S. et al. NanoLuc Complementation Reporter Optimized for Accurate Measurement of Protein Interactions in Cells. *ACS Chem. Biol.* **11**, 400–408 (2016).

30. Grover, R. K. et al. A Structurally Distinct Human Mycoplasma Protein that Generically Blocks Antigen-Antibody Union. *Science* **343**, 656–661 (2014).

31. Lim, S. L., Ichinose, H., Shinoda, T.& Ueda, H. Noncompetitive detection of low molecular weight peptides by open sandwich immunoassay. *Anal. Chem.* **79**, 6193–6200 (2007).

32. Takahashi, R., Yasuda, T., Ohmuro-Matsuyama, Y.& Ueda, H. BRET Q-Body: A Ratiometric Quench-based Bioluminescent Immunosensor Made of Luciferase-Dye-Antibody Fusion with Enhanced Response. *Anal. Chem.* **93**, 7571–7578 (2021).

33. Yasuda, T., Inoue, A., Kitaguchi, T.& Ueda, H. Rapid construction of fluorescence quenching-based immunosensor Q-bodies using α-helical coiled-coil peptides. *Chem. Commun.* **57**, 8206–8209 (2021).

34. Zhu, B. et al. Rapid and sensitive SARS-CoV-2 detection using a homogeneous fluorescent immunosensor Quenchbody with crowding agents. *Analyst* **147**, 4971–4979 (2022).

35. Yang, Y. H. et al. BRET Nano Q-Body: A Nanobody-Based Ratiometric Bioluminescent Immunosensor for Point-of-Care Testing. *ACS Sens.* **9**, 5955–5965 (2024).

36. Yazaki, S., Komatsu, M., Dong, J., Ueda, H.& Arai, R. Crystal Structures of Antigen-Binding Fragment of Anti-Osteocalcin Antibody KTM219. *Int. J. Mol. Sci.* **26**, 648 (2025).

37. Ohashi, H. et al. Insight into the Working Mechanism of Quenchbody: Transition of the Dye around Antibody Variable Region That Fluoresces upon Antigen Binding. *Bioconjug. Chem.* **27**, 2248–2253 (2016).

38. Cavanagh, J., Fairbrother, W. J., Palmer, A. G., Rance, M.& Skelton, N. J. Protein NMR Spectroscopy: Principles and Practice, 2nd Edition. *Protein NMR Spectroscopy: Principles and Practice, 2nd Edition*, 1–888 (2007).

39. Klein-Seetharaman, J. et al. Differential dynamics in the G protein-coupled receptor rhodopsin revealed by solution NMR. *Proc. Natl. Acad. Sci. USA* **101**, 3409–3413 (2004).

40. Eddy, M. T. et al. Extrinsic Tryptophans as NMR Probes of Allosteric Coupling in Membrane Proteins: Application to the A_{2A} Adenosine Receptor. *J. Am. Chem. Soc.* **140**, 8228–8235 (2018).

41. Jeong, H. J., Kawamura, T., Dong, J. H.& Ueda, H. Q-Bodies from Recombinant Single-Chain Fv Fragment with Better Yield and Expanded Palette of Fluorophores. *ACS Sens.* **1**, 88–94 (2016).

42. Mori, Y., Okumura, H., Watanabe, T.& Hohsaka, T. Antigen-dependent fluorescence response of anti-c-Myc Quenchbody studied by molecular dynamics simulations. *Chem. Phys. Lett.* **698**, 223–226 (2018).

43. Amit, A. G., Mariuzza, R. A., Phillips, S. E. V.& Poljak, R. J. 3-Dimensional Structure of an Antigen-Antibody Complex at 2.8-a Resolution. *Science* **233**, 747–753 (1986).

44. Piatesi, A., Aldag, C.& Hilvert, D. Switching antibody specificity through minimal mutation. *J. Mol. Biol.* **377**, 993–1001 (2008).

45. Dong, J. H. et al. PM Q-probe: A fluorescent binding protein that converts many antibodies to a fluorescent biosensor. *Biosens. Bioelectron.* **165**, 112425 (2020).

46. Kabsch, W. Xds. *Acta Cryst. D Biol. Crystallogr.* **66**, 125–132 (2010).

47. Evans, P. R.& Murshudov, G. N. How good are my data and what is the resolution? *Acta Cryst. D Biol. Crystallogr.* **69**, 1204–1214 (2013).

48. Emsley, P., Lohkamp, B., Scott, W. G.& Cowtan, K. Features and development of. *Acta Cryst. D Biol. Crystallogr.* **66**, 486–501 (2010).

49. Murshudov, G. N. et al. 5 for the refinement of macromolecular crystal structures. *Acta Cryst. D Struct. Biol.* **67**, 355–367 (2011).

50. Agirre, J. et al. The CCP4 suite: integrative software for macromolecular crystallography. *Acta Cryst. D Struct. Biol.* **79**, 449–461 (2023).

51. Laskowski, R. A., Macarthur, M. W., Moss, D. S.& Thornton, J. M. Procheck - a Program to Check the Stereochemical Quality of Protein Structures. *J. Appl. Crystallogr.* **26**, 283–291 (1993).

52. Lovell, S. C. et al. Structure validation by Cα geometry:: φ,ψ and Cβ deviation. *Proteins Struct. Funct. Genet.* **50**, 437–450 (2003).

53. Williams, C. J. et al. MolProbity: More and better reference data for improved all-atom structure validation. *Protein Sci.* **27**, 293–315 (2018).

54. Sali, A.& Blundell, T. L. Comparative Protein Modeling by Satisfaction of Spatial Restraints. *J. Mol. Biol.* **234**, 779–815 (1993).

55. Jorgensen, W. L., Chandrasekhar, J., Madura, J. D., Impey, R. W.& Klein, M. L. Comparison of Simple Potential Functions for Simulating Liquid Water. *J. Chem. Phys.* **79**, 926–935 (1983).

56. Maier, J. A. et al. ff14SB: Improving the Accuracy of Protein Side Chain and Backbone Parameters from ff99SB. *J. Chem. Theory Comput.* **11**, 3696–3713 (2015).

57. Joung, I. S.& Cheatham, T. E. Determination of alkali and halide monovalent ion parameters for use in explicitly solvated biomolecular simulations. *J. Phys. Chem. B* **112**, 9020–9041 (2008).

58. Salomon-Ferrer, R., Götz, A. W., Poole, D., Le Grand, S.& Walker, R. C. Routine Microsecond Molecular Dynamics Simulations with AMBER on GPUs. 2. Explicit Solvent Particle Mesh Ewald. *J. Chem. Theory Comput.* **9**, 3878–3888 (2013).

59. Darden, T., York, D.& Pedersen, L. Particle Mesh Ewald - an N.Log(N) Method for Ewald Sums in Large Systems. *J. Chem. Phys.* **98**, 10089–10092 (1993).

60. Andersen, H. C. Rattle - a Velocity Version of the Shake Algorithm for Molecular-Dynamics Calculations. *J. Comput. Phys.* **52**, 24–34 (1983).

61. McGibbon, R. T. et al. MDTraj: A Modern Open Library for the Analysis of Molecular Dynamics Trajectories. *Biophys. J.* **109**, 1528–1532 (2015).

Acknowledgements

We thank Dr. Eriko Nango from the Tohoku University for critical discussion on this work. This work was supported in part by JSPS KAKENHI (JP23K13607 to T.Y., JP19H02522 to R.A., JP18H03851 to H.U., and JP24K01264 to T.Kit.), the Sasakawa Scientific Research Grant from The Japan Science Society (2024-3031 to T.Y.), “Crossover Alliance to Create the Future with People, Intelligence, and Materials” from MEXT, Japan (JP2024Y008 to T.Y.), and the Cooperative Research Program of “Network Joint Research Center for Materials and Devices (MEXT)” (to R.A.). Synchrotron X-ray diffraction experiments were performed at Photon Factory (PF), KEK, under the approval of the PF program advisory committee (Proposal Nos. 2018G636, and 2020G658). We thank the beamline scientists and staff at PF, KEK.

Author contributions

T.Y., H.U., and T.Kit. conceived the project, designed the experiments. T.Y. and T.Kit. wrote the original manuscript. T.Y. and Y.U. performed plasmid construction, protein preparation, ELISA, and luminescence measurements. S.Y. and R.A. performed crystallization and X-ray structural analysis. T.Y., N.T., and H.Y. performed NMR study. T.Y. and M.T. performed MD simulation and its data analysis. B.Z. supported performing experiments. Y.U., M.T., N.T., H.Y., R.A., B.Z., and T.Kig. edited the manuscript. T.Kit. supervised the project. All authors have approved the final version of the manuscript.

Competing interests

T.Y., B.Z., H.U., and T.K. received honoraria from HikariQ Health, Inc. for another unrelated project.

Additional information

Supplementary information and supplementary movies accompanied this paper are available separately.